PAPER

CrossMark
click for updates

Combined experimental and computational approach to developing efficient photocatalysts based on Au/Pd–TiO$_2$ nanoparticles†

Alicja Mikolajczyk,[a] Anna Malankowska,[b] Grzegorz Nowaczyk,[c] Agnieszka Gajewicz,[a] Seishiro Hirano,[d] Stefan Jurga,[c] Adriana Zaleska-Medynska[b] and Tomasz Puzyn*[a]

Surface modified TiO$_2$-based nanoparticles (the so-called *second generation* nanoparticles) have unique semiconducting properties. They act as efficient photocatalysts, demonstrating catalytic activity under UV-vis and light-emitting diode (mix-LED) light. Consequently, they can be used as versatile, low-cost, clean and environmentally benign components in many innovative solutions, *e.g.* treatment technology for a wide range of environmental pollutants. However, for commercial application of TiO$_2$-based systems, it is crucial to develop nano-powders that can absorb light in the visible spectrum. Our investigation has demonstrated the potential benefits of using a chemoinformatics approach to obtaining knowledge on structural features responsible for the photocatalytic activity of second generation NPs under visible light. Through a combination of multiple linear regression (MLR) and a genetic algorithm (GA), we have developed a quantitative structure–properties relationship (Nano-QSPR) model (R^2 = 0.89, RMSE$_C$ = 1.67, Q_{LOO}^2 = 0.82, RMSE$_{CV}$ = 2.18, Q_{EXT}^2 = 0.80, RMSE$_P$ = 1.46) based on the most relevant physicochemical properties that characterized selected Au/Pd–TiO$_2$ NPs. According to the developed Nano-QSPR model, the anatase phase and palladium content are the main factors responsible for the higher activity of Au/Pd–TiO$_2$ photocatalysts under visible light. It should be noted that the methodology presented here can serve as an important starting point for further design of new nanomaterials with enhanced functionality, supported by chemoinformatics methods.

Environmental significance

Photocatalysis based on nano-catalysts is a very promising treatment technology for a variety of environmental pollutants because it is a low-cost, clean and environmentally friendly methodology. For commercial application of photocatalytic systems, it is crucial to develop nano-powders that can absorb visible light. In this work, based on combined experimental–theoretical studies, the structural features of Au/Pd@TiO$_2$ nanoparticles as well as the experimental conditions responsible for the increase in their photocatalytic activity under visible light were investigated. Importantly, the methodology presented here could be a substantial starting point for the further design of new nanomaterials with improved functionality without the necessity of performing expensive experimental studies.

[a] *Laboratory of Environmental Chemometrics, Faculty of Chemistry, University of Gdansk, Wita Stwosza 63, 80-308 Gdansk, Poland. E-mail: t.puzyn@qsar.eu.org*
[b] *Department of Environmental Technology, Faculty of Chemistry, University of Gdansk, Wita Stwosza 63, 80-308 Gdansk, Poland*
[c] *NanoBioMedical Center, Adam Mickiewicz University, Umultowska 85, 61-614 Poznan, Poland*
[d] *Center for Environmental Risk Research, National Institute for Environmental Studies, 16-2 Onogawa, Tsukuba, Ibaraki 305-8506, Japan*
† Electronic supplementary information (ESI) available. See DOI: 10.1039/c6en00232c

1. Introduction

Nanotechnology is the one of the fastest growing fields of science. Semiconductors, such as TiO$_2$-based nanomaterials, offer promising avenues for innovative applications as efficient photocatalysts. They offer an easy way of utilizing the energy of either natural sunlight or artificial indoor illumination.[1] Semiconductor-based heterogeneous photocatalysis is a versatile, low-cost, clean and environmentally benign treatment technology for a variety of environmental pollutants.[2–4] Modified TiO$_2$ nanoparticles (NPs) are the most investigated photocatalyst system.[5–7] It has been previously demonstrated that photocatalytic decomposition of a

This journal is © The Royal Society of Chemistry 2016

Environ. Sci.: Nano, 2016, 3, 1425–1435 | 1425

variety of organic and inorganic compounds in both gaseous and liquid phases using modified TiO_2 NPs, has potential application in sterilization, sanitation and air and water purification systems.[8–10] These photocatalysts can be used for photodegradation of pollutants both in gaseous form (e.g., removal of volatile organic compounds from the air) and in aqueous solutions (for example, removal of phenols from water and wastewater). They also enable the removal of odors from enclosed spaces, the inactivation of bacteria, hydrogen generation and photoconversion of CO_2 to light hydrocarbons.[4]

A serious drawback of titanium dioxide is that it can only be excited by ultraviolet light. This is the main limitation of using TiO_2-based photocatalysts in cheap and environmentally friendly methods of degradation of pollutants. TiO_2 reactivity in visible light ($\lambda > 400$ nm) can be achieved in several ways, through various structure/surface modifications:[11–16] (a) metal doping;[17–20] (b) non-metal doping;[21–23] (c) self-doping (reductive treatments);[24–30] (d) surface modifications by noble-metal nanoparticles of Ag, Au, Pt, and Pd;[31–43] (e) the use of dye-modified TiO_2[44–46] and (f) coupling TiO_2 with other semiconductors[47,48] (e.g., CdS).[49–52] In some cases, such doped or modified TiO_2 showed lower activity in the UV spectral range compared to the pristine TiO_2. Due to their optical and electronic structure-dependent properties, bimetallic nanoparticles (such as Au/Pd) seem to be a useful and promising type of metal nanoparticles used for TiO_2 modification, aimed at solar-driven environmental applications.[9] Therefore, the development of new photocatalysts exhibiting activity both under visible light and UV irradiation is crucial for broader commercial application of photocatalytic systems. However, the optimal amount and type of surface modifications influencing the efficiency of photocatalytic activity of second generation NPs under visible light are still unknown and experimental determination of features responsible for the photocatalytic activity of TiO_2-based NPs is often expensive and time-consuming. The development of photocatalysts exhibiting activity under visible light is crucial for broader commercial application of photocatalytic systems. The use of such photocatalysts will enable a new generation of renewable energy (solar radiation), allowing us to reduce the cost of the process and use it on the industrial scale. Without doubts, the physicochemical properties affecting the enhanced functionality of new, second generation nanoparticles should be evaluated. Thus, new methods for predicting photocatalytic activity are needed. Theoretical/computational methods can satisfy those needs.[53–55] One of the most promising approaches is the *quantitative structure–properties relationship* (QSPR) technique.[68–70] QSPRs are mathematical models quantitatively describing the relationship between the structure and the properties of chemicals. The successful concept and application of Nano-QSPR (here: QSPR for nanoparticles) has already been demonstrated, only for unmodified nanoparticles, the so-called first generation NPs, such as uncoated metal oxides, silver clusters, carbon nanotubes and fullerenes.[56–70]

As the second generation NPs have a higher degree of complexity and multifunctionality in comparison with the first generation NPs, more sophisticated methods that could express the complexity of such nanoparticles are needed. In the presented study, we applied Nano-QSPR to determine which structural features of Au/Pd–TiO_2 nanoparticles are responsible for their photocatalytic activity in the degradation of organic compounds under visible light irradiation. These aspects are crucial to designing TiO_2-based photocatalysts efficient under visible light, to be used in environmental science and technology.

2. Materials and methods

2.1. Preparation and characterisation of Au/Pd–TiO_2 photocatalysts

Nanoparticles of titanium dioxide modified with Au and Pd metal clusters were obtained by hydrolysis of titanium(IV) isopropoxide (TIP) in a water/dioctylsulfosuccinate sodium salt (AOT)/cyclohexane microemulsion containing Au and Pd precursors in water cores. Mixing was carried out for 1 h under nitrogen; Au and Pd were then reduced by dropwise addition of a microemulsion containing the reducing agent (hydrazine). The titanium isopropoxide was added into the microemulsion system containing the Au and Pd nanoparticles. The microemulsions were mixed and purged with nitrogen, washed, dried and calcined for 3 h at different temperatures, as described previously.[35,36] The size, shape and composition of the nanoparticles were studied using Cs-corrected STEM with EDX. The most important characteristics of the synthesized TiO_2 modified structures are summarized in Fig. 1 and Table 1. More details on the characterization of the materials used can be found in the ESI† (S1. Materials, S2. XRD details, and Fig. S1).

2.2. Measurement of photocatalytic activity under visible light (the endpoint)

The photocatalytic activity of the prepared samples was estimated by measuring the decomposition rate of a 0.21 mM phenol aqueous solution in the presence of visible radiation. The aqueous phase contained 125 mg of the photocatalyst, 24 cm^3 of deionized water and 1 cm^3 of phenol (Co = 500 mg dm^{-3}). The prepared suspension was stirred and aerated in the dark, and the contents of the reactor were photoirradiated with a 1000 W xenon lamp (Oriel). The optical path included a water filter and a glass filter (GG 420) that blocked wavelengths shorter than 420 nm. The phenol concentration was estimated by a colorimetric method using a UV-vis spectrophotometer (DU-7, Beckman).[35]

2.3. Comparative measurement of photocatalytic activity under UV-vis and mix-LED light

The investigation of photocatalytic activity under UV-vis and mix-LED light was carried out to establish whether the surface modification of TiO_2 does not really decrease
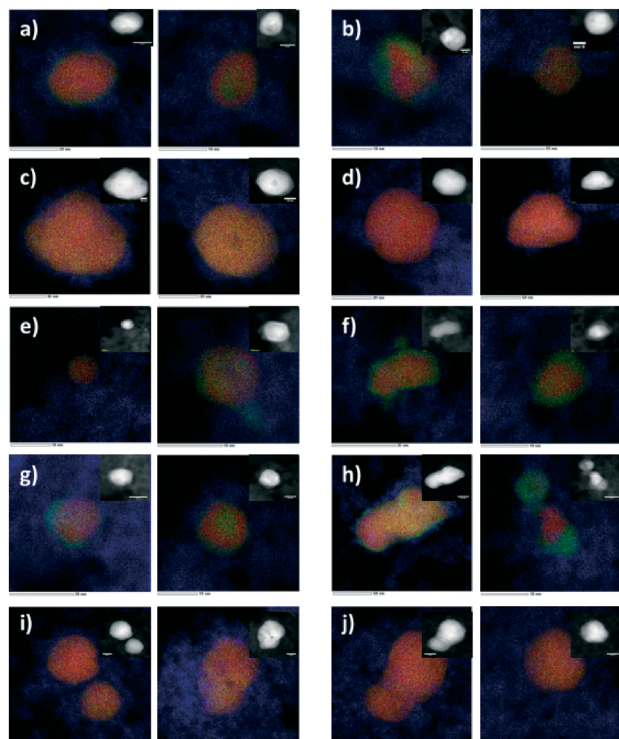
Fig. 1 HAADF images with z-contrast combined with mapping images of bimetallic Au/Pd nanoparticles deposited onto TiO₂ with different Pd and/or Au amounts/ratios and calcined at 400 °C: (a) 0.1Pd_0.1Au, (b) 0.1Pd_0.25Au, (c) 0.1Pd_0.5Au, (d) 0.1Pd_1.25Au, (e) 0.5Pd_0.1Au, (f) 0.5Pd_0.25Au, (g) 0.5Pd_0.5Au, (h) 0.25Pd_0.25Au, (i) 0.25Pd_0.5Au, and (j) 0.25Pd_1.25Au (blue is Ti, red is Au and green is Pd).

photocatalytic activity in this range of light (mixed LEDs, λ_{max} = 415 and 375 nm). The measurement details pertaining to the photocatalytic activity under visible, UV-vis and mix-LED light are summarized in Table S1.† The photocatalytic activity of TiO₂ modified with Au, Pd and Au/Pd nanoparticles was determined in the process of cleaning volatile organic compounds (VOC) from air under 25 mixed LEDs (5 LEDs, λ_{max}= 375 nm and 20 LEDs, λ_{max}= 415 nm) as the irradiation source. Toluene (Co = 200 ppm) was used as a model air contaminant. The suspension of the photocatalyst in water was loaded as a thick film onto a glass plate using the painting technique and subsequently dried. A flat stainless steel reactor (V = 30 cm³) was equipped with a quartz window, two valves and a septum.[70] After the valves were closed, the reactor was kept in the dark for 15 min and the contents of the reactor were photoirradiated. The toluene concentration in the gas phase was measured using gas chromatography (Clarus 500, PerkinElmer).[36] The photocatalytic activity of the prepared samples was estimated by measuring the decomposition rate of a 0.21 mM phenol aqueous solution in the presence of UV-vis radiation. The aqueous phase contained 125 mg of the photocatalyst, 24 cm³ of deionized water and 1 cm³ of phenol (Co = 500 mg dm⁻³). The prepared suspension was stirred and aerated in the dark, and the contents of the reactor were photoirradiated with a 1000 W Xenon lamp

(Oriel). The optical path included a water filter and a glass filter (GG 420) that blocked wavelengths shorter than 420 nm. The phenol concentration was estimated by a colorimetric method using a UV-vis spectrophotometer (DU-7, Beckman).[35] All details pertaining to the structure, size, calcination temperature and photocatalytic activity are reported in the ESI† (Table S2, Fig. S1–S7).

2.4. Descriptors

The quantitative structure–properties relationship (Nano-QSPR) modeling of nanoparticles was performed to identify the structural factors responsible for the photocatalytic activity of the second generation NPs. In the developed Nano-QSPR model, we used a set of 27 structural descriptors. This included 17 empirical descriptors (the so-called "0D nano-descriptors") and 10 theoretical "liquid-drop-model"-derived descriptors[65] that quantitatively described the variability in nanoparticle structure (Table 2; for the values, please refer to Tables S2 and S3 in the ESI†).[55,71,72]

2.5. Nano-QSPR model development and validation

In order to develop the Nano-QSPR model,[68–69] we applied the multiple regression method (MLR)[73] combined with a genetic algorithm (GA)[74] implemented in QSARINS 2.0 software.[75] MLR is a standard regression technique, in which the endpoint (here: photocatalytic activity under vis light, %τ_{PhOH}) is described as the best combination of the most relevant auto-scaled nano-descriptors used as independent variables ($x_1, x_2 \ldots x_n$) (eqn (1) and Fig. 2):

$$\%\tau_{PhOH} = b_0 + b_1x_1 + b_2x_2 + \ldots + b_nx_n \quad (1)$$

According to the golden standards of QSPR modeling, every model should be externally validated.[76] This means that the predictive ability of the model should be assessed based on predictions performed for nanoparticles that have not been previously used for calibrating the model. In order to do that, the dataset was split on the basis of a 1 : X algorithm[77] into two sets: the training set (to be used for developing the Nano-QSPR model) and the validation set (to be used only for validating the model's predictive ability). To perform the split, we sorted the nanoparticles by increasing the value of %τ_{PhOH}. Then, every second NP was attributed to the validation set, whereas the remaining NPs formed the training set (Fig. 2).

We used the squared correlation coefficient (R^2) and the root-mean-square error of calibration (RMSE_C) as the measures of the goodness-of-fit for the developed model. To reduce the probability of overfitting, prove the robustness of the Nano-QSPR model and verify the stability of the model, an internal validation procedure was performed. For this purpose, we applied the cross-validated coefficient Q_{LOO}^2 (leave-one-out method) and the root-mean-square error of cross-validation RMSE_CV.[78] To demonstrate the external predictivity of the model, we used the concordance correlation coefficient

This journal is © The Royal Society of Chemistry 2016

Environ. Sci.: Nano, 2016, **3**, 1425–1435 | **1427**

Table 1 Experimental characteristics of the nanoparticles used in the study (samples calcined at 400 °C)

| Sample label | Amount of noble metal precursor [mol%] | | SBET, $m^2 \, g^{-1}$ | LSPR, λ_{max} [nm] | Range of size of NPs [nm] | The structure (alloy, core–shell or monometallic) of noble metal nanoparticles seated at the surface of TiO₂* |
	Pd	Au				
Pure TiO₂	0	0	154	—	—	
0.1Au	0	0.1	168	572	8–31	
0.25Au	0	0.25	139	574	12–63	
1.25Au	0	1.25	140	572	12–129	
0.1Pd	0.1	0	154	428	4–4.5	
0.25Pd	0.25	0	182	432	4–11	
0.1Pd_0.1Au	0.1	0.1	156	536	8–45	
0.1Pd_0.25Au	0.1	0.25	157	590	6–25	
0.1Pd_0.5Au	0.1	0.5	148	684	63–140	
0.1Pd_1.25Au	0.1	1.25	179	614	54–200	
0.25Pd_0.25Au	0.25	0.25	159	548	17–170	
0.25Pd_0.5Au	0.25	0.5	158	590	7–70	
0.25Pd_1.25Au	0.25	1.25	145	616	16–68	
0.5Pd_0.1Au	0.5	0.1	136	438	5–17	
0.5Pd_0.25Au	0.5	0.25	164	462	15–35	
0.5Pd_0.5Au	0.5	0.5	153	504	19–40	
0.5Pd_1.25Au	0.5	1.25	139	614	8–80	

(CCC), external validation coefficient Q_{Ext}^2, root-mean-square error of prediction (RMSEP), and mean absolute error (MAE).[76,79,82] All the model statistics were calculated according to the equations presented in the ESI† (Table S3). The externally validated model, for which the values of the corresponding correlation coefficients (R^2, Q_{LOO}^2, Q_{BOOT}^2, Q_{Ext}^2 and CCC) and the errors (RMSE$_C$, RMSE$_{CV}$ and RMSE$_P$) are of similar range, can be regarded as well-fitted, sufficiently robust and of high predictive ability. Thus, the model can be used for performing valuable predictions for new nanoparticles. For the description of the statistical parameters towards the development of the Nano-QSPR model, please refer to the ESI,† Table S4.

3. Results and discussion

3.1. Nano-QSPR model

The developed Nano-QSPR model utilized two descriptors (Table 3 and eqn (2)):

$$\%\tau_{PhOH} = 7.21 + 4.87(\pm0.58)XRD_{anatase} + 2.44(\pm0.58)Pd_{\%mol} \quad (2)$$

and was characterized by the following statistical characteristics: $R^2 = 0.89$, RMSE$_C$ = 1.67, $R_{adj}^2 = 0.88$, $R^2 - R_{adj}^2 = 0.02$, $Q_{BOOT}^2 = 0.96$, $Q_{LOO}^2 = 0.82$, RMSE$_{CV}$ = 2.18, $Q_{EXT}^2 = 0.80$, $R_{EXT}^2 = 0.82$, RMSE$_P$ = 1.46, CCC = 0.90, MAE$_{EXT}$ = 1.05, F = 40.16, $p > 0.05$ and $n = 17$.

According to Roy et al.,[82] the determination of the threshold value for the error measure in the external validation (MAE$_{EXT}$) should be checked using the following criteria: (i) good prediction can be expected if MAE ≤ 0.1 × training set range and MAE + 3 × σ ≤ 0.2 training set range; (ii) bad prediction can be expected if MAE > 0.15 × training set range or MAE + 3 × σ > 0.25 training set range; and (iii) moderate quality can be expected if it does not fall under either of the described conditions. For the developed Nano-QSPR model (eqn (2)), MAE$_{EXT}$ is equal to 0.14, the training range is 1.28, while the MAE$_{EXT}$ + 3 × σ is 0.51. The best prediction can be expected if MAE$_{EXT}$ ≤ 0.13 and MAE$_{EXT}$ + 3 × σ ≤ 0.26 and bad prediction can be expected if MAE > 0.19 or MAE + 3 × σ > 0.32. Since the prediction fulfills the described conditions only in part (0.13 < MAE < 0.19 and 0.26 < MAE + 3 × σ > 0.32), the prediction can be considered to be of moderate quality. Another important parameter, which simply verifies how small the differences between the experimental data and external data set predictions are, is the concordance correlation coefficient (CCC). The CCC measures both precision (how far the observations are from the fitting line) and accuracy (how far the regression line deviates from the slope of the line passing through the origin, i.e. the concordance line). Consequently, any divergence of the regression line from the concordance line gives a CCC value of less than 1 as a result. Thus, the CCC calculated for our model indicates that the predictive ability is high.

1428 | Environ. Sci.: Nano, 2016, 3, 1425–1435

This journal is © The Royal Society of Chemistry 2016

Table 2 List of descriptors used for Nano-QSPR model development

Symbol	Description	Units	Type of descriptor
$Pd_{\%mol}$	Amount of Pd precursor	[mol%]	Experimentally-based "0D" descriptors
$Au_{\%mol}$	Amount of Au precursor	[mol%]	
S_{BET}	BET surface area	[m^2 g^{-1}]	
DRS	Max peak from DRS spectra	[nm]	
LSPR, λ_{max}	Surface plasmon resonance	[nm]	
$Size_{min}$	Minimum size of NPs	[nm]	
$Size_{max}$	Maximum size of NPs	[nm]	
$Size_{average}$	Average size of NPs	[nm]	
$\nu^{core-shell}$	Core–shell structure of bimetallic cluster	[a.u.]	
ν^{alloy}	Alloy structure of bimetallic cluster	[a.u.]	
Mw	Molecular weight for $Au_{\%mol}$ or $Pd_{\%mol}$	[g mol^{-1}]	
$XRD_{Anatase}$	Typical diffraction peaks X-ray diffraction measurements corresponding to the anatase phase	[a.u.]	
$XRD_{Brookite}$	Typical diffraction peaks X-ray diffraction measurements corresponding to the brookite phase	[a.u.]	
XRD_{Au}	Typical diffraction peaks X-ray diffraction measurements corresponding to the gold molecule	[a.u.]	
$2\theta\ max_{Anatase}$	Range of 2θ derived from XRD spectra for the	[°]	
$2\theta\ min_{Anatase}$	presence of anatase phase	[°]	
$2\theta\ max_{Brookite}$	Range of 2θ derived from XRD spectra for the	[°]	
$2\theta\ min_{Brookite}$	presence of brookite phase	[°]	
$2\theta\ max_{Metallic\_Au}$	Range of 2θ derived from XRD spectra for the	[°]	
$2\theta\ min_{Metallic\_Au}$	presence of gold atoms	[°]	
$\bar{r}_{Winger-Seitz}$	Average Wigner–Seitz radius	[nm]	Descriptors derived from the "Liquid drop" model
$d_{V/r}^{min}$	Surface-to-volume ratio for $Size_{min}$	[nm]	
$d_{V/r}^{max}$	Surface-to-volume ratio for $Size_{max}$	[nm]	
$d_{V/r}^{average}$	Surface-to-volume ratio for $Size_{average}$	[nm]	
r_S^{min}	Ratio of surface molecules for $Size_{min}$	[nm]	
r_S^{max}	Ratio of surface molecules for $Size_{max}$	[nm]	
$r_S^{average}$	Ratio of surface molecules for $Size_{average}$	[nm] descriptors	
η^{min}	Number of elementary particles for $Size_{min}$	[a.u]	
η^{max}	Number of elementary particles for $Size_{max}$	[a.u]	
$\eta^{average}$	Number of elementary particles for $Size_{average}$	[a.u]	

Please note that the coefficients provided in eqn (2) have been derived for the normalized values of descriptors. The mean values ($\bar{x}_j$) of $XRD_{anatase}$ and $Pd_{\%mol}$ were 3793.77 and 0.23, respectively. The standard deviations (s_j) were equal to 377.98 and 0.18. The detailed procedure of the normalization is described in the ESI,† Table S4. This means that at the data pre-processing stage, the mean values and the standard deviations were calculated for each descriptor. Then, the mean value of a given descriptor was subtracted from the descriptor value for each nanoparticle and the result was divided by the standard deviation. In effect, all descriptors were transformed into the same scale (scale of standard deviations, the so-called 'Z-scale') and the same order of magnitude. The model indicates that there are two important factors ($XRD_{anatase}$ and $Pd_{\%mol}$) influencing the photocatalytic activity of modified TiO$_2$ NPs under visible light. According to the values of standardized regression coefficients (eqn (2)), the contribution of the intensity of a diffraction peak corresponding to the anatase phase is more important than the Pd content. The influence of the $XRD_{anatase}$ descriptor on the modeled variable (%τ_{PhOH}) is about 50% higher than that of the Pd content.

The developed model (eqn (2)) has been thoroughly validated according to the OECD QSAR validation principles.[23]

Only a properly validated model can offer a meaningful mechanistic interpretation.[81] The graphical representation of the correlation between the observed (experimental) values of %τ_{PhOH} and the predicted values from the developed Nano-QSPR model is presented in Fig. 3a. The plot of the standardized cross-validated residuals (%τ_{PhOH}^{obs} − %τ_{PhOH}^{pred}) vs. leverage values (Williams plot) is presented in Fig. 3b. This plot confirms that all training and validation compounds were located within the applicability domain (i.e., the area defined by the structural similarity of nanoparticles to the training set, where the predictions are reliable). All NPs were characterized to have sufficient similarity to the training set (the leverage values $h_i < h^* = 0.75$). Moreover, there were no outlying predictions (i.e. with residuals differing by more than 3 standard deviations from the average residual value for %τ_{PhOH}^{obs} − %τ_{PhOH}^{pred}). Therefore, no outlying results with respect to either the structural similarity or the activity predictions were obtained for the investigated TiO$_2$-based samples. In addition, the applicability domain has been verified by using the basic theory of the standardization approach, as proposed by Roy et al.[80] The standardization approach is a simple method for defining the X-outliers (in the case of the training set) and identifying the compounds that reside outside the domain (in the case of the validation set).[80] The
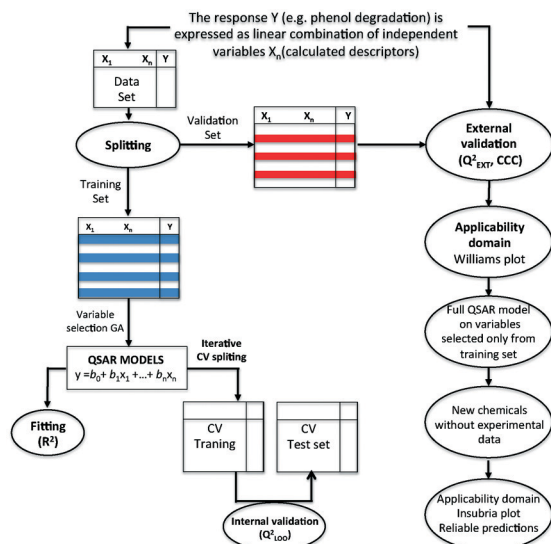
Fig. 2 The idea of the QSPR method. Column y contains known values of the property of interest or the set of observations. Matrix X contains molecular nano-descriptors for all observations. By developing the quantitative dependence between known endpoint values and corresponding descriptors, one can calculate the unknown values in column y (*i.e.* $\%\tau_{PhOH}$).

obtained results (Fig. 3b and Table S5, ESI†) indicated that there are no outliers in the case of both the training and validation sets. Thus, both methods (the leverage and the standardization approaches) led to the same conclusions.

We have additionally performed the Y-scrambling numerical experiment to avoid defining the correlation by chance and to confirm the significance of the developed Nano-QSPR model.[74] We built 500 models (the so-called "random models") utilizing the same descriptors ($XRD_{anatase}$ and

$Pd_{\%mol}$) but correlated them with the photocatalytic activity ($\%\tau_{PhOH}$) data randomly shuffled every time. Based on the calculations of the $RMSE_C$ and $RMSE_{CV}$ values for these models, we were able to determine the minimal error that can be calculated without the presence of any model. Since the values of both $RMSE_C$ and $RMSE_{CV}$ were about two times lower than those for the random models (Fig. S8, ESI†), we have confirmed the significance of the developed Nano-QSPR model (eqn (2)). This confirms that the model has not been obtained by a chance correlation.

The comprehensive validation of the model itself and of its applicability domain proved the high predictive ability of Nano-QSPR for modeling the photocatalytic activity of nano-sized Au/Pd–TiO$_2$. Thus, the interpretation of the selected descriptors brought significant insight into the current knowledge of structural and physicochemical factors most likely to affect the $\%\tau_{PhOH}$ values of nanoparticle systems of interest.

3.2. Mechanistic interpretation

To understand the mechanism behind the photocatalytic activity of the Au/Pd–TiO$_2$ nanoparticles, the selected descriptors of the model should be analyzed and interpreted. Titanium dioxide can exist in three polymorphic forms: anatase (stable), brookite (metastable), and rutile (most stable). All these polymorphs exhibit different properties and consequently different photocatalytic activities. Thus, in this study, the properties of each polymorphic structure of Au/Pd–TiO$_2$ were examined (Table 2 and Fig. S6†).

One of the two descriptors utilized by the Nano-QSPR model (eqn (2)) is $XRD_{anatase}$. It is a descriptor derived from X-ray diffraction measurements of bimetallic Au/Pd–TiO$_2$ NPs representing the intensity of a diffraction peak of the anatase

Table 3 Descriptors selected for the model and the modeled endpoint values

| Nanoparticle | Descriptors | | Efficiency of phenol degradation % τ_{PhOH} [%][b] | | Set[a] |
	Pd, %mol	XRD spectra	Observed	Predicted	
Pure TiO$_2$	0.00	3483.3	1.01	0.31	T
0.1Pd_1.25Au	0.10	3328.1	1.30	0.29	T
0.1Au	0.00	3581.5	1.60	1.53	P
0.5Pd_0.1Au	0.50	3116.7	1.70	2.37	T
0.1Pd_0.5Au	0.10	3684.8	2.30	4.12	T
0.1Pd_0.25Au	0.10	3963.3	5.90	7.55	P
0.25Pd_0.5Au	0.25	3887.2	5.90	8.59	T
0.25Pd_0.25Au	0.25	3762.9	6.20	7.06	T
0.5Pd_1.25Au	0.50	3240.9	6.60	3.91	P
0.25Au	0.00	4155.8	7.10	8.61	T
0.25Pd_1.25Au	0.25	3596.6	8.20	5.00	T
1.25Au	0.00	4163.8	8.80	8.71	P
0.1Pd_0.1Au	0.10	4112.7	9.60	9.40	T
0.5Pd_0.25Au	0.50	3879.2	10.70	11.78	T
0.1Pd	0.10	4204.9	11.30	10.54	P
0.5Pd_0.5Au	0.50	3935.3	13.40	12.48	T
0.25Pd	0.25	4582.6	19.20	17.17	T

[a] T – training set, P – validation (test) set. [b] The efficiency of phenol degradation after 1 h of irradiation under visible light [%].
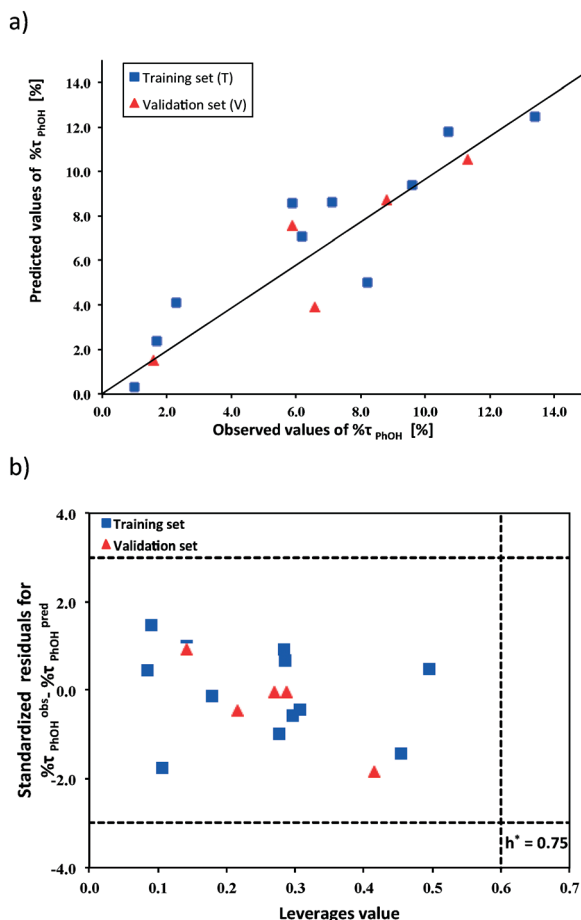
1430 | *Environ. Sci.: Nano*, 2016, **3**, 1425–1435

This journal is © The Royal Society of Chemistry 2016

a)

b)

Fig. 3 a) Plot of the experimentally determined (observed) *vs.* predicted values of %τ_{PhOH} b) plot of the standardized cross-validated residuals *vs.* the leverage values (Williams plot) describing the domain of applicability of the GA-MLR model. The dashed lines represent the residual threshold (0 ± 3 standard deviation units), and h^* represents the critical leverage value.

phase (the intensity of the peak describes the prevalence of one type of polymorphic form over the others). The significance of the XRD$_{anatase}$ descriptor indicated that the major phase responsible for the efficiency of phenol degradation under visible light is the anatase form. Analysis of the XRD data (shown in Fig. 4), indicated that the typical diffraction peaks which correspond to anatase ($2\theta = 25, 38, 48, 55, 63, 69$) were exhibited by all samples (Fig. S6†).[83] These results prove that anatase is the major phase that influences phenol degradation in the studied Au/Pd–TiO$_2$ samples.

The second descriptor represents the amount of Pd precursor in Au/Pd–TiO$_2$ samples (Pd$_{\%mol}$). The photocatalytic activity of the NPs increases with increasing values of Pd$_{\%mol}$. Interestingly, the influence of the XRD$_{anatase}$ descriptor on the modelled variable is about 30% higher than that of Pd%, *i.e.* the prevalence of the anatase phase in TiO$_2$-based samples is much more important for the photocatalytic activity compared to the Pd content.

Our results are in agreement with the literature findings.[84,85] For example, Luttrell *et al.*[85] indicated that anatase

is the most active phase among the existing TiO$_2$ structures (*i.e.* brookite, rutile, anatase). Meanwhile, Li *et al.*[84] have shown that its high photocatalytic activity is directly connected to the prolonged lifetime of charge carriers and spatial charge separation. Thus, the highest photocatalytic activity of the anatase phase can be related to the band gap of anatase of ~3.2 eV, compared with ~3.0 eV for rutile.[9,25] Obviously, the difference in the band gap energy is due to structural differences. The Ti–Ti distances in the anatase structure are greater than in rutile, whereas, the Ti–O distances are shorter. These structural differences change the mass density and lead to difference in the electronic configuration. The rutile phase is 9% more dense than the anatase, presenting more pronounced localization of 3d orbitals and therefore a narrower 3d band gap than anatase. In addition, the O 2p and Ti 3d hybridizations are different for both structures. These differences influence the partial density of state (PDOS) and consequently determines different band gaps of both structures. As indicated by Setiawati and Kawano,[86] the photocatalytic performance of anatase generally is considered superior to that of the more stable rutile. This is attributed to a higher density of localized states and consequent surface-adsorbed hydroxyl radicals and slower charge carrier recombination in anatase relative to rutile parameters that contribute to improved performance.[85–88] Thus, utilization of the XRD$_{anatase}$ descriptor in the developed Nano-QSPR model confirmed the results described by several laboratory groups.[85,86,89] The results presented in eqn (2) prove that new photocatalysts with surface modification (second generation NPs should be synthesized based on the anatase TiO$_2$ phase.

The second descriptor used in the developed Nano-QSPR model (Pd$_{\%mol}$) provides the quantitative answer to the question of which component of Au/Pd–TiO$_2$ determines variability in nanomaterial activity under visible light. The descriptor clearly shows positive correlation between the increasing amount of Pd atoms in the bimetallic cluster adsorbed on the surface of TiO$_2$ NPs and the efficiency of phenol degradation. Interestingly, descriptors that correspond to the Au content (see Table S2†) have not been selected by the genetic algorithm as significant contributors to the model. It could be concluded that the amount of Pd in bimetallic clusters, which influences the TiO$_2$ structure changes, is the major factor determining phenol degradation under visible light.

As mentioned, the illumination of TiO$_2$ causes photogenerated holes and electrons to migrate to the surface, where they oxidize or reduce species, respectively. However, the recombination of the charge carriers causes a noticeable reduction in the photoactivity. The immobilization of noble metal nanoparticles has been used to inhibit this recombination wherein the photogenerated electrons are trapped in the immobilized noble metal, improving the photocatalytic activity. There is a number of studies describing that reactivity of TiO$_2$ under visible light can be achieved by surface modifications using noble-metal nanoparticles (*i.e.* Au, Ag,
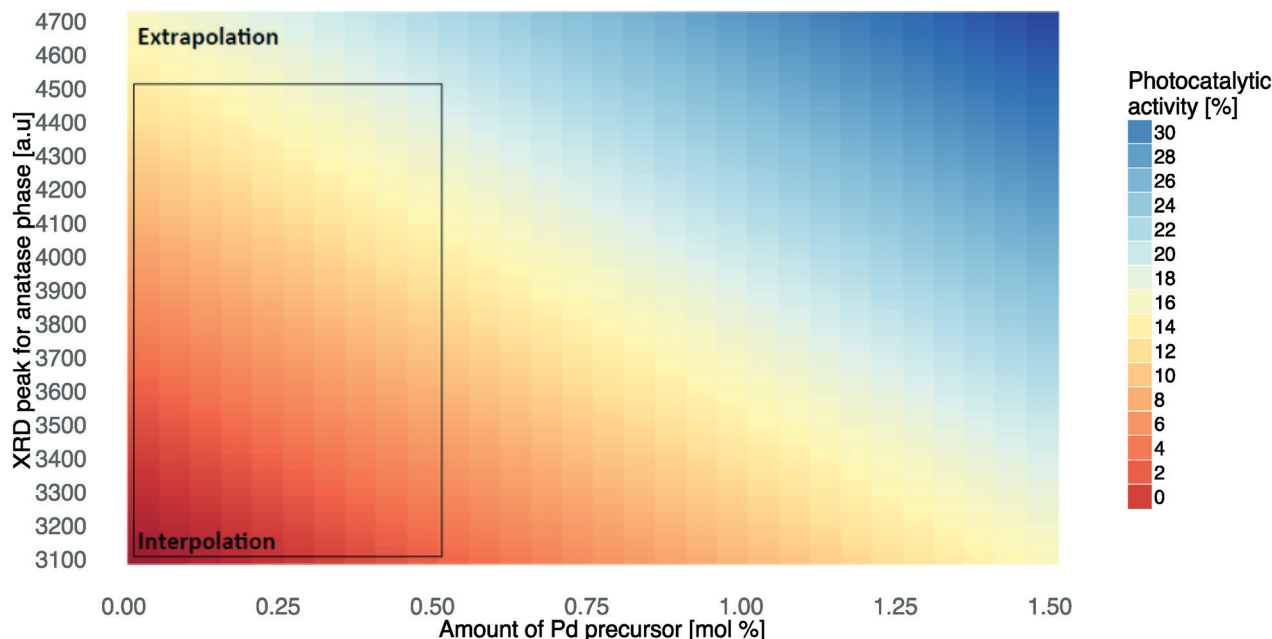
This journal is © The Royal Society of Chemistry 2016

Environ. Sci.: Nano, 2016, **3**, 1425–1435 | **1431**

Fig. 4 Simulation of photocatalytic activity under visible light based on $XRD_{anatase}$ and $Pd_{\%mol}$ descriptors.

Pd, Pt).[9] Overall, the high activity is attributable to the structure of the bimetallic nanoparticles, as well as their composition. These results have been confirmed by the developed Nano-QSPR model (eqn (2)) that utilized both features related to the structure of the TiO_2 sample ($XRD_{anatase}$) and their modifications ($Pd_{\%mol}$).

It must also be pointed out that the role of noble metals in TiO_2 excitation is different under UV and visible light. Under UV irradiation, TiO_2 is activated in the first step and photo-generated electrons are trapped by noble metal nanoparticles, hindering the recombination of charge carriers (e^-/h^+), which results in the activity increase.[90] In contrast, under visible light irradiation the photons are absorbed by metallic NPs through their localized surface plasmon resonance (LSPR) excitation, followed by electron transfer from plasmonically excited noble metal nanoparticles to the conduction band (CB) of titania and consecutively to adsorbed oxygen.[37,91]

In this context, we conclude that bimetallic nanoparticles containing higher amounts of Pd can accept electrons more effectively, as Pd has a larger work function than Au (*i.e.* minimum energy or thermodynamic work needed to remove an electron from a solid to a vacuum outside the solid surface). It can be expected that the Pd content influences the interphase charge transfer within the nanomaterial, which greatly facilitates the flow of valence electrons from the metal to TiO_2 and promotes phenol degradation. Moreover, in both types of nanoparticle formation (Au-core/Pd-shell and three-layer core/shell), the greatest photocatalytic activity is observed for samples with shells containing primarily Pd (Fig. S7†). These observations are in agreement with various experiments. For instance, Mizukoshi *et al.*[89] reported that core/

shell particles containing more Pd show a higher promotional effect on TiO_2 photocatalytic activities. It could be expected that in the case of core/shell particles with a higher Pd content, the thicker Pd shell is supposed to effectively shield photogenerated electrons from recombination with holes. From the photocatalytic point of view, the presence of palladium atoms at the surface of Au/Pd nanoparticles on TiO_2 is more favourable than the presence of gold atoms.[9] According to Sarkany *et al.*,[92] the Au/Pd molar ratio of 20/80 in core/shell structured nanoparticles exhibited the highest catalytic activity. These findings are in agreement with our experimental results; by microscopic analysis, we revealed that the ratio of the noble metals (Au and Pd) strongly affected the structure of the BNPs and the photocatalytic activity (Table 1, Fig. 1, and Fig. S7†). A higher ratio of Pd to Au (Pd > Au) resulted in the formation of Au_{core}/Pd_{shell} structures (Table 1 and Fig. 1). In the opposite situation, where the samples had a higher ratio of gold to palladium (Au > Pd), alloy nanoparticles were formed. Both Au-core/Pd-shell and three-layer core/shell nanoparticle types were observed when the Au/Pd ratio was 1:1. Tanaka *et al.*[39] reported that the effectiveness of degradation under visible light irradiation is related to the type of functionalized core–shell gold–palladium particles supported on TiO_2 (Au@Pd/TiO_2). Mizukoshi *et al.*[89] reported that Au-core/Pd-shell bimetallic nanoparticles have shown superior catalytic activities for the hydrogenation of olefins compared with a mixture of Au and Pd monometallic nanoparticles, because of the relatively positive charge of the Pd-shell structure. The Mizukoshi group concluded that this is possibly due to the electrical affinity of the double bonds of organic pollutants adsorbed on the positively charged Pd surface.[89]

1432 | *Environ. Sci.: Nano*, 2016, **3**, 1425–1435

This journal is © The Royal Society of Chemistry 2016

3.3. Application of the developed nano-QSPR model in environmental science and technology

In order to estimate and visualize the predicted values outside of the applicability domain, we have systematically applied the model (eqn (2)) to simulate the values of photocatalytic activity under visible light ($\%\tau_{PhOH}$) to different combinations of the descriptors: $XRD_{anatase}$ and $Pd_{\%mol}$. In other words, the values of $\%\tau_{PhOH}$ may be predicted using either interpolation (within the range of the training set) or extrapolation (outside of the training set). Although extrapolation by definition is less reliable, the observed trends are quite clear. Thus, valuable conclusions might be formulated based on the extrapolated data. The interpolated and extrapolated regions are indicated in Fig. 4. It is worth noting that the developed property map (Fig. 4) is a useful tool to simulate the relationship between $XRD_{anatase}$/$Pd_{\%mol}$ features and photocatalytic activity under visible light which could be used to reach an efficiency equal to the photocatalytic activity achieved under UV-vis and mix-LED irradiation (Table 1).

More importantly, the methodology presented here, which is based on chemoinformatics, is a significant starting point for the design of new photocatalysts with improved functionality. However, the predictions based on the currently presented model (eqn (2) and Fig. 4) would be reliable only assuming that (i) the designed structures are similar enough to those used for training the model and (ii) the photocatalytic activity is measured under the same environmental conditions (temperature, presence of a specific metal, other compounds, *etc.*) as the experimental data used this study.

In addition, the limitations of the developed Nano-QSPR model should be taken into account. These limitations are related to the Pd concentration, which can be used during synthesis in a water-in-oil (W/O) microemulsion system as well as for controlling the ratio of the TiO_2 phases. The solubility and stability of the Pd precursor depend on the synthesis method and on the resulting adsorption surface area of TiO_2. Moreover, the values of the peak intensities that correspond to the polymorphs of TiO_2 are dependent on several factors: the number of unit cells in a unit volume, wavelength, temperature, absorbent agents, *etc.* Thus, when planning prospective experimental studies for further quantitative Nano-QSPR modelling, more experimental details that characterize the surface and crystal structures of modified TiO_2 NPs should be considered.

Still, the Nano-QSPR approach presented here might be applied as a preliminary step in designing new second generation nanoparticles with desired properties, *i.e.* in chemoinformatics-based environmental engineering. TiO_2 photocatalysts become more and more widely used in the field of environmental technology, as they possess many advantages, such as high photocatalytic activity, excellent stability, non-toxicity to human beings, and a low cost. TiO_2-based nanoparticles have a number of photocatalytic applications, including self-cleaning surfaces, anti-fogging surfaces, solar cells, water disinfection and visible light-sensitive materials

for pollutants degradation, hydrogen evolution by water splitting, and CO_2 conversion to hydrocarbon fuels. Small-scale photocatalytic systems with artificial UV light have already been in the market for several years, whereas solar photocatalytic water treatment plants are in the demonstration phase and pilot projects for drinking water purification systems in developing countries have only just started.

Taking into account the potential application of surface-modified TiO_2 NPs, as well as the necessary characterisation of NPs, novel, fast, and inexpensive chemoinformatics-based environmental engineering procedures for the characterisation and design of efficient second generation nanomaterials are needed. Therefore, the developed Nano-QSPR model which quantitatively describes the relationship between photocatalytic activity under visible light and the structure of surface-modified TiO_2 based NPs can be recommended for further application in *in silico* design of novel second generation nanoparticles. The proposed model is the first step in the development of a series of computational tools to predict the physico-chemical properties of second generation nanoparticles.

Conclusions

This study presents the first-ever quantitative structure–properties relationship (Nano-QSPR) model, which identifies and describes the features responsible for the photocatalytic activity under visible light of second generation nanoparticles (*i.e.* Au/Pd–TiO2 NPs). The combined experimental–theoretical study has demonstrated that the anatase phase and palladium content are the main factors responsible for the higher activity of Au/Pd–TiO_2 photocatalysts under visible light. We believe that the methodology presented here can serve as an important starting point for the further design of new photocatalysts with enhanced functionality supported by computational approaches.

Acknowledgements

This journal is © The Royal Society of Chemistry 2016

Environ. Sci.: Nano, 2016, **3**, 1425–1435 | **1433**

References

1 Y. Li, W. Zhang, J. Niu and Y. Chen, *ACS Nano*, 2012, **6**, 5164–5173.

2 A. Fujishima and K. Honda, *Nature*, 1972, **238**, 37–38.

3 M. A. A. Aziz, A. A. Jalil, S. Triwahyono and A. Ahmad, *Green Chem.*, 2015, **17**, 2647–2663.

4 M. Kaushik and A. Moores, *Green Chem.*, 2016, **18**, 622–637.

5 M. Kapilashrami, Y. Zhang, Y.-S. Liu, A. Hagfeldt and J. Gu, *Chem. Rev.*, 2014, **114**, 9662–9707.

6 D. Fattakhova-Rohlfing, A. Zaleska and T. Bein, *Chem. Rev.*, 2014, **114**, 9487–9558.

7 J. Schneider, M. Matsuoka, M. Takeuchi, J. Zhang, Y. Horiuchi, M. Anpo and D. W. Bahnemann, *Chem. Rev.*, 2014, **114**, 9919–9998.

8 R. Konaka, E. Kasahara, W. C. Dunlap, Y. Yamamoto, K. C. Chien and M. Inoue, *Free Radical Biol. Med.*, 1999, **27**, 294–300.

9 A. Fujishima, T. N. Rao and D. A. Tryk, *J. Photochem. Photobiol., C*, 2000, **1**, 1–21.

10 K. Hashimoto, H. Irie and A. Fujishima, *Jpn. J. Appl. Phys.*, 2005, **44**, 16.

11 M. Pelaez, N. T. Nolan, S. C. Pillai, M. K. Seery, P. Falaras, A. G. Kontos, P. S. M. Dunlop, J. W. J. Hamilton, J. A. Byrne, K. O'shea, M. H. Entezari and D. D. Dionysiou, *Appl. Catal., B*, 2012, **125**, 331–349.

12 M. Pini, R. Rosa, P. Neri, F. Bondioli and A. M. Ferrari, *Green Chem.*, 2015, **17**, 518–531.

13 D. Walsh, N. M. Sanchez-Ballester, K. Ariga, A. Tanaka and M. Weller, *Green Chem.*, 2015, **17**, 982–990.

14 R. Altenburger, H. Walter and M. Grote, *Environ. Sci. Technol.*, 2004, **38**, 6353–6362.

15 M. Li, M. E. Noriega-Trevino, N. Nino-Martinez, C. Marambio-Jones, J. Wang, R. Damoiseaux, F. Ruiz and E. M. V. Hoek, *Environ. Sci. Technol.*, 2011, **45**, 8989–8995.

16 A. Al-Kattan, A. Wichser, S. Zuin, Y. Arroyo, L. Golanski, A. Ulrich and B. Nowack, *Environ. Sci. Technol.*, 2014, **48**, 6710–6718.

17 J. Reszczynska, A. Iwulska, G. Sliwinski and A. Zaleska, *Physicochem. Probl. Miner. Process.*, 2012, **48**, 201–208.

18 J. Reszczyńska, T. Grzyb, J. W. Sobczak, W. Lisowski, M. Gazda, B. Ohtani and A. Zaleska, *Appl. Surf. Sci.*, 2014, **307**, 333–345.

19 S. W. Bae, P. H. Borse, S. J. Hong, J. S. Jang and J. S. Lee, *J. Korean Phys. Soc.*, 2007, **51**, 22–26.

20 M. Maeda and T. Yamada, *J. Phys.: Conf. Ser.*, 2007, **61**, 755–759.

21 A. Zaleska, E. Grabowska, J. W. Sobczak, M. Gazda and J. Hupka, *Appl. Catal., B*, 2009, **89**, 469–475.

22 A. Zaleska, J. W. Sobczak, E. Grabowska and J. Hupka, *Appl. Catal., B*, 2008, **78**, 92–100.

23 T. Ohno, T. Mitsui and M. Matsumura, *Chem. Lett.*, 2003, **32**, 364–365.

24 K. Sasan, F. Zuo, Y. Wang and P. Feng, *Nanoscale*, 2015, **7**, 13369–13372.

25 X. Zhou, F. Yang, B. Jin, Y. Huang and Z. Wu, *Mater. Lett.*, 2013, **112**, 145–148.

26 F. Zuo, L. Wang and P. Feng, *Int. J. Hydrogen Energy*, 2014, **39**, 711–717.

27 X. Liu, H. Xu, L. R. Grabstanowicz, S. Gao, Z. Lou, W. Wang, B. Huang, Y. Dai and T. Xu, *Catal. Today*, 2014, **225**, 80–89.

28 Y. Yang, T. Zhang, L. Le, X. Ruan, P. Fang, C. Pan, R. Xiong, J. Shi and J. Wei, *Sci. Rep.*, 2014, **4**, 7045.

29 L.-B. Xiong, J.-L. Li, B. Yang and Y. Yu, *J. Nanomater.*, 2012, 831524.

30 F. Zuo, L. Wang, T. Wu, Z. Zhang, D. Borchardt and P. Feng, *J. Am. Chem. Soc.*, 2010, **132**, 11856–11857.

31 A. Zielińska-Jurek and J. Hupka, *Catal. Today*, 2014, **230**, 181–187.

32 Z. Mandegani, M. Asadi, Z. Asadi, A. Mohajeri, N. Iranpoor and A. Omidvar, *Green Chem.*, 2015, **17**, 3326–3337.

33 M. Cinelli, S. R. Coles, M. N. Nadagouda, J. Blaszczynski, R. Slowinski, R. S. Varma and K. Kirwan, *Green Chem.*, 2015, **17**, 2825–2839.

34 Y. Z. Chen, G. R. Cai, Y. M. Wang, Q. Xu, S. H. Yu and H. L. Jiang, *Green Chem.*, 2016, **18**, 1212–1217.

35 A. Cybula, J. B. Priebe, M.-M. Pohl, J. W. Sobczak, S. Matthias, A. Zielińska-Jurek, A. Brückner and A. Zaleska, *Appl. Catal., B*, 2014, **152–153**, 202–211.

36 A. Cybula, G. Nowaczyk, M. Jarek and A. Zaleska, *J. Nanomater.*, 2014, 918607.

37 A. Gołąbiewska, W. Lisowski, M. Jarek, G. Nowaczyk, A. Zielińska-Jurek and A. Zaleska, *Appl. Surf. Sci.*, 2014, **317**, 1131–1142.

38 P. Kittisakmontree, H. Yoshida, S.-I. Fujita, M. Arai and J. Panpranot, *Catal. Commun.*, 2015, **58**, 70–75.

39 A. Tanaka, S. Sakaguchi, K. Hashimoto and H. Kominami, *ACS Catal.*, 2013, **3**, 79–85.

40 Y. Shiraishi, K. Fujiwara, Y. Sugano, S. Ichikawa and T. Hirai, *ACS Catal.*, 2013, **3**, 312–320.

41 A. Gallo, M. Marelli, R. Psaro, V. Gombac, T. Montini, P. Fornasiero, R. Pievo and V. Dal Santo, *Green Chem.*, 2012, **14**, 330–333.

42 A. Gallo, T. Montini, M. Marelli, A. Minguzzi, V. Gombac, R. Psaro, P. Fornasiero and V. Dal Santo, *Green Sustainable Chem.*, 2012, **5**, 1800–1811.

43 R. Su, R. Tiruvalam, A. J. Logsdail, Q. He, C. A. Downing, M. T. Jensen, N. Dimitratos, L. Kesavan, P. P. Wells, R. Bechstein, H. H. Jensen, S. Wendt, R. Catlow, C. J. Kiely, G. J. Hutchings and F. Besenbacher, *ACS Nano*, 2014, **8**, 3490–3497.

44 D. Jiang, D. Wu and Y. Sun, *J. Solid State Chem.*, 2008, **181**, 593–602.

45 K. S. Yao, T. C. Cheng, S. J. Li, L. Y. Yang, K. C. Tzeng, C. Y. Chang and Y. Ko, *Surf. Coat. Technol.*, 2008, **203**, 922–924.

46 D. Chatterjee, S. Dasgupta and N. Rao N, *Sol. Energy Mater. Sol. Cells*, 2006, **90**, 1013–1020.

47 A. Franco, M. C. Neves, M. M. L. Ribeiro Carrott, M. H. Mendonca, M. I. Pereira and O. C. Monteiro, *J. Hazard. Mater.*, 2009, **161**, 545–550.

1434 | *Environ. Sci.: Nano*, 2016, **3**, 1425–1435

This journal is © The Royal Society of Chemistry 2016

48 P. Wang, D. Li, J. Chen, X. Zhang, J. Xian, X. Yang, X. Zheng, X. Li and Y. Shao, *Appl. Catal., B*, 2014, **160–161**, 217–226.

49 M. Zhong, J. Shi, F. Xiong, W. Zhang and C. Li, *Sol. Energy*, 2012, **86**, 756–763.

50 X. Li, T. Xia, C. Xu, J. Murowchick and X. Chen, *Catal. Today*, 2014, **225**, 64–73.

51 M. Marchelek, B. Bajorowicz, P. Mazierski, A. Cybula, T. Klimczuk, M. Winiarski, N. Fijałkowska and A. Zaleska, *Catal. Today*, 2015, **252**, 47–53.

52 B. Bajorowicz, A. Cybula, M. J. Winiarski, T. Klimczuk and A. Zaleska, *Molecules*, 2014, **19**, 15339–15360.

53 A. Mikolajczyk, A. Gajewicz, B. Rasulev, N. Schaeublin, E. Maurer-Gardner, S. Hussain, J. Leszczynski and T. Puzyn, *Chem. Mater.*, 2015, **27**, 2400–2407.

54 A. Gajewicz, N. Schaeublin, B. Rasulev, S. Hussain, D. Leszczynska, T. Puzyn and J. Leszczynski, *Nanotoxicology*, 2014, **0**, 1–13.

55 T. Puzyn, D. Leszczynska and J. Leszczynski, *Small*, 2009, **5**, 2494–2509.

56 A. Gajewicz, T. Puzyn, B. Rasulev, D. Leszczynska and J. Leszczynski, *Nanosci. Nanotechnol.–Asia*, 2011, **1**, 53–58.

57 A. Gajewicz, B. Rasulev, T. C. Dinadayalane, P. Urbaszek, T. Puzyn, D. Leszczynska and J. Leszczynski, *Adv. Drug Delivery Rev.*, 2012, **64**, 1663–1693.

58 A. Gajewicz, N. Schaeublin, B. Rasulev, S. Hussain, D. Leszczynska, T. Puzyn and J. Leszczynski, *Nanotoxicology*, 2014, **1**, 1–13.

59 A. Gajewicz, N. Schaeublin, B. Rasulev, S. Hussain, D. Leszczynska, T. Puzyn and J. Leszczynski, *Nanotoxicology*, 2015, **9**, 313–325.

60 T. Puzyn, D. Leszczynska and J. Leszczynski, *Small*, 2009, **5**, 2494–2509.

61 T. Puzyn, A. Mostrag-Szlichtyng, A. Gajewicz, M. Skrzynski and A. P. Worth, *Struct. Chem.*, 2011, **22**, 795–804.

62 T. Puzyn, B. Rasulev, A. Gajewicz, X. Hu, T. P. Dasari, A. Michalkova, H. M. Hwang, A. Toropov, D. Leszczynska and J. Leszczynski, *Nat. Nanotechnol.*, 2011, **6**, 175–178.

63 N. Sizochenko, K. Jagiello, J. Leszczynski and T. Puzyn, *J. Phys. Chem. C*, 2015, **119**, 25542–25547.

64 N. Sizochenko, V. Kuz'min, L. Ognichenko and J. Leszczynski, *J. Mater. Chem. Eng.*, 2016, **54**, 698–706.

65 N. Sizochenko, B. Rasulev, A. Gajewicz, V. Kuz'min, T. Puzyn and J. Leszczynski, *Nanoscale*, 2014, **6**, 13986–13993.

66 N. Sizochenko, B. Rasulev, A. Gajewicz, E. Mokshyna, V. E. Kuz'min, J. Leszczynski and T. Puzyn, *RSC Adv.*, 2015, **5**, 77739–77745.

67 J. Liu, Y. S. Hwang and J. J. Lenhart, *Environ. Sci.: Nano*, 2015, **2**, 528–540.

68 J. C. Dearden, *Org. React.*, 2016, **1**, 1–44.

69 K. Roy, S. Kar and R. N. Das, *Understanding the basics of QSAR for applications in pharmaceutical sciences and risk assessment*, Academic press, 2015.

70 T. Puzyn, J. Leszczynski and M. T. Cronin, *Recent advances in QSAR studies: methods and applications*, Springer Science & Business Media, 2010.

71 M. Nischk, P. Mazierski, M. Gazda and A. Zaleska, *Appl. Catal., B*, 2014, **144**, 674–685.

72 G. Oberdörster, A. Maynard, K. Donaldson, V. Castranova, J. Fitzpatrick, K. Ausman, J. Carter, B. Karn, W. Kreyling, D. Lai, S. Olin, N. Monteiro-Riviere, D. Warheit and H. Yang, *Part. Fibre Toxicol.*, 2005, **2**, 8.

73 M. H. Kutner, *Applied linear regression models*, McGraw-Hill/Irwin, 2004.

74 J. Holland, *Adaptation in Natural and Artificial Systems*, MIT Press, Michigan, 1992.

75 P. Gramatica, N. Chirico, E. Papa, S. Cassani and S. Kovarich, *J. Comput. Chem.*, 2013, **34**, 2121–2132.

76 P. Gramatica and A. Sangion, *J. Chem. Inf. Model.*, 2016, **56**, 1127–1131.

77 M. Hewitt, M. T. D. Cronin, J. C. Madden, P. H. Rowe, C. Johnson, A. Obi and S. J. Enoch, *J. Chem. Inf. Model.*, 2003, **47**, 1460–1468.

78 A. Tropsha, P. Gramatica and V. K. Gombar, *QSAR Comb. Sci.*, 2003, **22**, 69–77.

79 N. Chirico and P. Gramatica, *J. Chem. Inf. Model.*, 2011, **51**, 2320–2335.

80 K. Roy, S. Kar and P. Ambure, *Chemom. Intell. Lab. Syst.*, 2015, **145**, 22–29.

81 *Guidance Document on the Validation of (Quantitative) Structure–Activity Relationship(Q)SARs Models, ENV/JM/MONO(2007)2*, Paris, France, 2007.

82 K. Roy, R. N. Das, P. Ambure and R. B. Aher, *Chemom. Intell. Lab. Syst.*, 2016, **152**, 18–33.

83 R. M. Mohamed and E. S. Baeissa, *Appl. Catal., A*, 2013, **464–465**, 218–224.

84 G. H. Li and K. A. Gray, *Chem. Phys. Lett.*, 2007, **339**, 173–187.

85 T. Luttrell, S. Halpegamage, J. Tao, A. Kramer, E. Sutter and M. Batzill, *Sci. Rep.*, 2014, **4**, 4043.

86 E. Setiawati and K. Kawano, *J. Alloys Compd.*, 2008, **451**, 293–296.

87 Q. H. Zhang, L. Gao and J. K. Guo, *Int. J. Inorg. Mater.*, 2000, **15**, 556–560.

88 Q. H. Zhang, L. Gao and J. K. Guo, *Appl. Catal., B*, 2000, **26**, 207–215.

89 Y. Mizukoshi, K. Sato, T. J. Konno and N. Masahashi, *Appl. Catal., B*, 2010, **94**, 248–253.

90 Z. B. Hai, N. El Kolli, D. B. Uribe, P. Beaunier, M. Jose-Yacaman, J. Vigneron, A. Etcheberry, S. Sorgues, C. Colbeau-Justin, J. F. Chena and H. Remita, *J. Mater. Chem. A*, 2013, **1**, 10829–10835.

91 A. Zielińska-Jurek, *J. Nanomater.*, 2014, 1–17.

92 A. Sarkany, P. Hargittai and A. Horvath, *Top. Catal.*, 2007, **46**, 121–128.

This journal is © The Royal Society of Chemistry 2016

Environ. Sci.: Nano, 2016, **3**, 1425–1435 | **1435**